Systematic analysis of RNAi-accessible SARS-CoV-2 replication steps identifies ORF1 as promising target

Shubhankar Ambike[1,*], Cho-Chin Cheng[1,*], Suliman Afridi[1], Martin Feuerherd[1], Philipp Hagen[1], Vincent Grass[1], Olivia Merkel[2], Andreas Pichlmair[1,3], Chunkyu Ko[1] and Thomas Michler[1,3,#]

[1] Institute of Virology, Technische Universität München / Helmholtz Zentrum München, Trogerstr. 30, 81675 Munich, Germany

[2] Department of Pharmacy, Pharmaceutical Technology and Biopharmaceutics, Ludwig-Maximilians-Universität München, Butenandtstraße 5, 81377 Munich, Germany

[3] German Center for Infection Research (DZIF), Munich partner site, Germany

[*] These authors contributed equally

[#] Correspondence: thomas.michler@tum.de (T.M.)

A promising approach to tackle the Severe Acute Respiratory Syndrome Coronavirus-2 (SARS-CoV-2) could be to use small interfering (si)RNAs[1-4]. However, the proof of concept that SARS-CoV-2 can be targeted with siRNAs is missing. Here, we report that siRNAs can target genomic RNA (gRNA) of SARS-CoV-2 after cell entry, terminating replication before start of transcription and preventing cytopathic effects. Coronaviruses replicate via negative sense intermediate transcripts using a unique discontinuous transcription process[5,6]. As a result, each viral RNA contains identical sequences at the 5' and 3' end[7]. While negative replication intermediates were inaccessible for siRNAs, targeting sequences shared by different viral transcripts allowed simultaneous suppression of gRNA and subgenomic (sg)RNAs. However, siRNAs which targeted open reading frame 1 (ORF1), which is solely contained in gRNA[7], showed a higher antiviral efficacy. We show that an increased accessibility of translational-active ORF1 before the start of transcription, in combination with the out-competition of siRNAs targeting common regions of transcripts by highly abundant sgRNAs, were responsible for this. Our work encourages the development of siRNA-based therapies for SARS-CoV-2 and suggests that early therapy start, together with targeting ORF1, might be key for high antiviral viral efficacy.

Research Square

Preprints are preliminary reports that have not undergone peer review. They should not be considered conclusive, used to inform clinical practice, or referenced by the media as validated information.

32 SARS-CoV-2 is causing a pandemic with so far unforeseeable consequences on global
33 health, politics and economy. SARS-CoV-2, like other coronaviruses affecting humans, is
34 mainly transmitted via respiratory secretions[8] and replicates primarily in respiratory
35 epithelial cells[9]. Due to its lytic cell cycle[10], it causes severe endothelial injury and
36 widespread microangiopathy[11], which can result in respiratory failure and death. While
37 some progress has been made by repurposing the RNA polymerase inhibitor
38 Remdesivir[12] or by ameliorating SARS-CoV-2 induced lung injury using Dexamethason[13],
39 lethality of COVID-19 remains high[14]. A promising alternative approach could be to deliver
40 siRNAs to respiratory tract by inhalation[15] and induce degradation of viral RNAs by the
41 RNA-interference (RNAi) machinery. Studies performed with SARS-CoV-1 or Middle East
42 Respiratory Syndrome Coronavirus (MERS-CoV), showed that siRNAs can silence viral
43 RNA and relieve symptoms caused by related coronaviruses[16-20]. However, while several
44 publications proposed siRNAs as potential therapeutic also for COVID-19[1,2,21,22], until
45 today there is no proof that SARS-CoV-2 can be inhibited by siRNAs, not to mention a
46 systematic analysis which replication steps are accessible for RNAi.
47 SARS-CoV-2, as other coronaviruses, has a positive sense, single-stranded RNA
48 genome with a length of approximately 30,000 nucleotides. Following binding to the
49 cellular receptor angiotensin-converting enzyme 2[23], the virus is taken up via
50 endocytosis[24]. After fusion with the endosomal membrane[25], the ribonucleocapsid is
51 released into the cytoplasm. Here, the viral genome serves as template for initial
52 translation of the polyprotein 1ab (pp1b) from ORF1 by the cellular ribosomal machinery.
53 Pp1ab is cleaved into 16 non-structural proteins (NSPs) of which several assemble
54 around the viral genome to form the replication/transcription complex (RTC)[26]. As for
55 other positive sense RNA viruses, transcription does not take place in the cytosol, but
56 exclusively within double-membrane vesicles[27]. Therefore, the viral RTC associates with
57 endoplasmic reticulum membranes to form so-called viral replication organelles (ROs).
58 Here, the viral genome serves as template for transcription of full-length progenitor gRNA
59 as well as sgRNAs encoding for structural (S, envelope protein [E], membrane protein
60 [M], Nucleocapsid [N]) as well as accessory proteins (3a, 6, 7a, 7b, 8 and 10)[7]. As a
61 results of the discontinuous transcription[5,6], each coronaviral RNA contains an identical
62 3´ (the ~70 nucleotides long leader sequence [L]) as well as 5' end (N ORF and 3´

63 untranslated region [3´UTR])[7]. Next, sgRNAs are released from ROs[28], translated into the
64 corresponding protein and gRNA packaged by the structural proteins to assemble
65 progeny virions.
66 Coronaviruses protect their RNA well. Besides the envelope and capsid protecting virions,
67 nucleocapsid proteins bind directly to the viral genome. Thus, even between uncoating
68 and incorporation into double-membraned ROs, the genome is not present as naked
69 RNA[29]. Furthermore, while sgRNAs are exported from ROs for translation, this does not
70 seem to be the case for gRNA which remains associated with double-membraned
71 vesicles[28]. Currently, it is not clear whether the different viral RNA species produced
72 during replication are accessible for an RNAi-based therapy. Furthermore, certain viral
73 components might be essential for replication, whereas the suppression of others might
74 be tolerated by the virus. Thus, suppression of reporter constructs as often performed
75 during siRNA development might not accurately predict the effect of siRNAs on viral
76 replication and spread. To shed light upon these questions, we systematically analysed
77 which steps of the SARS-CoV-2 life cycle can be targeted by siRNA and how this would
78 affect viral replication.

79

80 Following the events in viral replication cycle, first, we investigated whether siRNAs can
81 directly target the genome of SARS-CoV-2 after cell entry. We chose ORF1 as target
82 region, as it is only contained in full-length genomic, but not sgRNAs[7]. We individually
83 transfected three siRNAs which were active in previous luciferase reporter screens
84 (Supplementary Fig. 2a) into VeroE6 cells. After 16h, cells were infected with a
85 recombinant SARS-CoV-2, expressing Green Fluorescent Protein (GFP) from a
86 sequence integrated at the ORF7 locus (rSARS-CoV-2-GFP)[30]. Viral infection and spread
87 was monitored by quantifying GFP^+ cells every 4h over the course of three days (Fig. 1a,
88 top). Importantly, as the ORF1-specific siRNAs do not target the transcript from which
89 GFP is expressed, a suppression of GFP expression would indicate that siRNAs targeted
90 full-length gRNA (Fig. 1a, bottom). Indeed, we found the number of GFP^+ cells reduced
91 to approximately 50% by each of the tested siRNAs (Fig. 1b-d). Importantly, this
92 difference was already present at the earliest time point (12h post infection [p.i.]) with
93 detectable GFP signal (Fig. 1b), indicating that genomes of incoming virus were

successfully targeted. We confirmed this by repeating the experiment using *wildtype* SARS-CoV-2, but lysed cells 24h p.i. and quantified SARS-CoV-2 gRNA by reverse-transcriptase quantitative PCR (RT-qPCR). As indicated by our first experiment, gRNA was reduced in groups pre-treated with the ORF1-specific siRNAs (Fig. 1e). To further confirm that indeed genomes of incoming virus were degraded, we transfected cells with a pool of three ORF1-specific siRNAs 6h before infection with *wildtype* SARS-CoV-2 and quantified intracellular viral RNAs at different time points. Viral RNAs were further differentiated into full-length gRNA and sgRNAs (see methods for details). We found that gRNA was reduced as early as 1h p.i. (Fig. 1f), before sgRNAs were synthesized (Fig. 1g). Treatment with ORF1-specific siRNAs prevented sgRNA expression (Fig. 1g), reduced morphologic changes (Fig. 1h), and improved metabolic rate of cells (Fig.1i). Taken together, our data proves that siRNAs can target the genome of SARS-CoV-2 and terminate viral replication at an early replication step preventing cytopathy.

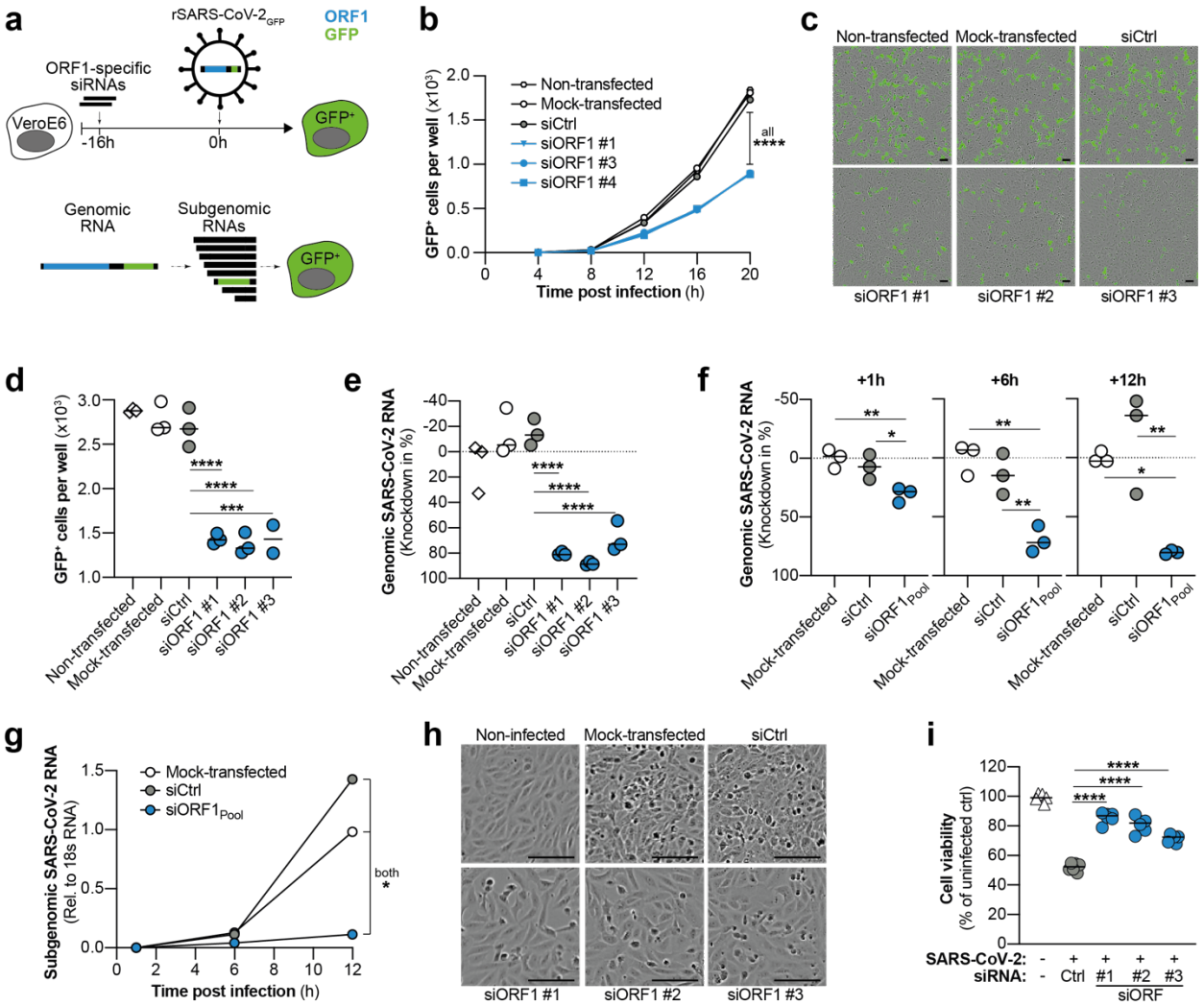

Fig. 1 | Effect of targeting genomic SARS-CoV-2 RNA with siRNAs on viral replication and cell viability. a, top, Experimental setup used in **b-d**. VeroE6 cells were transfected with siRNAs targeting ORF1 (siORF1) 16h before infection with recombinant, GFP-expressing SARS-CoV-2 (rSARS-CoV-2-GFP) and number of GFP$^+$ positive cells quantified. **a, bottom**, Schematic representation of gRNA, as well as sgRNAs. Note that ORF1 (blue) is only part of full-length gRNA but not sgRNAs. GFP, Green Fluorescent Protein. **b**, Kinetic of viral spread showing number of GFP$^+$ cells determined by automated quantification using the integrated Incucyte S3 software. **c-d**, GFP expression 24h after infection with rSARS-CoV-2-GFP. **c**, Exemplary fluorescence microscopy pictures. Bar at lower right indicates 0.1 mm length and (**d**) quantification of GFP$^+$ cells. **e**, Same experimental setup as in **b-d** but cells were infected with *wildtype* SARS-CoV-2 and lysed after 24h to quantify genomic SARS-CoV-2 RNA from cell lysate by RT-qPCR. **f-g**, siRNAs used in **b-e** were pooled and transfected into VeroE6 cells 6h before infection with *wildtype* SARS-CoV-2. Cells were lysed at different time points after infection and SARS-CoV-2 (**f**) gRNA as well as (**g**) sgRNAs quantified by RT-qPCR. **h-I**, VeroE6 cells were transfected with siRNAs 6h before infection with *wildtype* SARS-CoV-2 and 24h later (**h**) phase contrast microscopy pictures taken. Bar at lower right indicates 0.1 mm length. **i**, Cell viability determined by measuring conversion from resazurin to resorufin using a fluorometer. **b-g,** Mean of triplicates for each treatment group is shown. Bars in **d-f,i** show median. Statistical differences were calculated using (**b,c**) Repeated Measures One-Way Anova or (**d-f,i**) regular One-Way Anova with Dunnett´s multiple comparison correction. *, p<0.05; **, p<0.01; ***, p<0.001; ****, p<0.0001

Currently it is unclear if both, negative and positive sense coronaviral RNA, or only RNA with a certain polarity is accessible for RNAi silencing. This question is particularly interesting when designing therapeutic siRNAs, as potentially both strands of the siRNA

129 could convey antiviral activity. To gain a more detailed understanding on the kinetic of
130 RNA synthesis during SARS-CoV-2 replication, we lysed *wildtype* SARS-CoV-2-infected
131 VeroE6 cells at different time points. Positive and negative sense viral RNAs were
132 individually quantified by strand specific first strand synthesis (see Methods). Negative
133 sense gRNA was detected in low quantities already 1h p.i., but strongly increased at 6h
134 p.i. when it was more abundant than positive sense gRNA (Fig. 2a). In contrast, sgRNAs
135 started to appear only at 6h p.i. (Fig. 2b). Consistent with other coronaviruses, lower
136 amounts of negative sense sgRNAs were detected as compared to their positive sense
137 counterparts[31]. We now investigated whether negative sense SARS-CoV-2 RNA is
138 accessible for RNAi-mediated silencing. We developed siRNAs that specifically targeted
139 either negative or positive sense SARS-CoV-2 RNA. We chose the N ORF as target
140 region, as it is also part of sgRNAs which are – in contrast to gRNA – exported from ROs[28]
141 and should therefore be easily accessible for siRNAs. siRNA strand-specific activity was
142 validated by co-transfecting siRNAs with reporter plasmids expressing either the positive
143 or negative sense N coding sequence incorporated downstream to *Renilla* luciferase
144 gene (see scheme in Fig. 2c and methods). The majority of siRNAs showed high
145 selectivity against the RNA strand they were designed (Supplementary Fig. 1). We chose
146 siRNAs with almost exclusive activity against either the positive or negative sense
147 reporter (Fig. 2d). To our surprise, only siRNAs active against positive sense N ORF
148 succeeded in reducing sgRNA of *wildtype* SARS-CoV-2 (Fig. 2e), thereby inhibiting viral
149 spread in the rSARS-CoV-2-GFP model (Fig. 2f). In summary, our data prooves that
150 negative sense SARS-CoV-2 RNAs are inaccessible for RNAi.

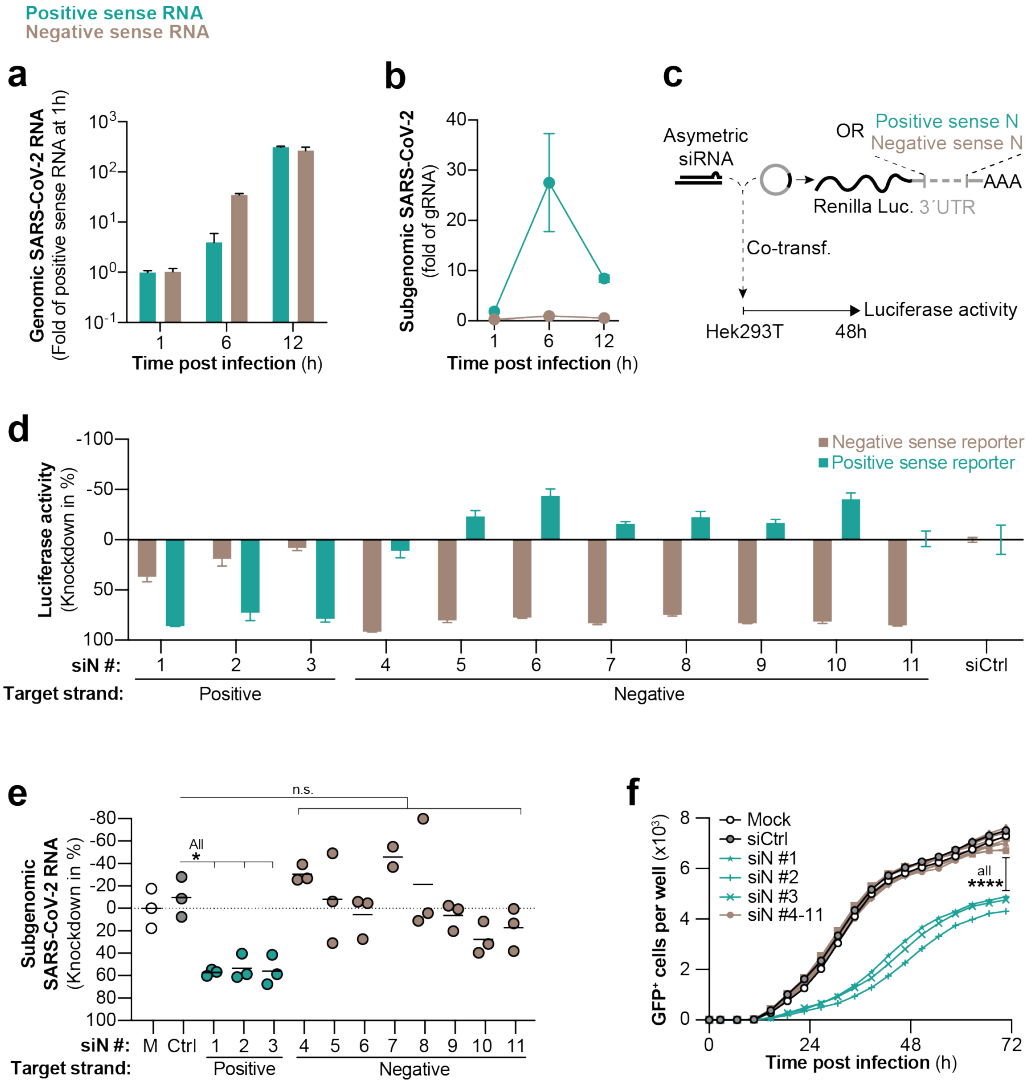

Fig.2 | Evaluation of SARS-CoV-2 negative sense RNA as siRNA target. a-b, Kinetics of negative and positive sense SARS-CoV-2 RNAs following *wildtype* SARS-CoV-2 infection of VeroE6 cells. Negative and positive sense RNAs were individually transcribed to cDNA by using either poly A or poly T primers and (**a**) gRNA and (**b**) sgRNAs quantified by RT-qPCR. **c**, Experimental setup to determine siRNA sense specific activities. Luciferase reporters with incorporated positive or negative sense N sequences in the 3´UTR of R*enilla* luciferase were co-transfected with siRNAs and (**d**) 48h later luciferase activity measured. **e**, siRNAs were transfected into VeroE6 cells 6h before infection with *wildtype* SARS-CoV-2 and 24h p.i. sgRNAs quantified from cell lysate using RT-qPCR; M = Mock-transfected. **f**, Same setup as in **e**, but VeroE6 cells were infected with rSARS-CoV-2-GFP and GFP⁺ cells quantified every 4h. Graphs in **a-b,d-e** show mean and error bars SEM. Statistical differences were calculated using (**e**) Regular or (**f**) Repeated Measures One-Way Anova with Dunnett´s multiple comparision correction. n.s., non significant, *, p<0.05; ****, p<0.0001

162 We further investigated whether targeting the common regions shared by all SARS-CoV-
163 2 transcripts (L, N ORF and 3´UTR; Fig. 3a) would allow simultaneous suppression of
164 gRNA as well as sgRNAs. In contrast to inceptive experimental setup, we infected VeroE6
165 cells with *wildtype* SARS-CoV-2 and afterwards transfected siRNAs targeting either the
166 common regions of transcripts (shown in red) or ORF1 (blue) which is contained only in
167 gRNA. For each target region, we used a pool of three siRNAs which previously showed
168 similar activities against luciferase reporters (Supplementary Fig. 2a). As expected,
169 ORF1-specific siRNAs suppressed only gRNA, wheareas siRNAs targeting common
170 regions of transcripts suppressed gRNA and sgRNAs (Fig. 3b). We next investigated how
171 targeting sgRNAs in addition to gRNA would affect antiviral efficacy. Therefore, we
172 infected VeroE6 cells with rSARS-CoV-2-GFP and 3h later, individually transfected three
173 siRNAs for each target region. Viral spread was evaluated by quantifying GFP^+ cells every
174 4h over a course of three days. All tested siRNAs reduced GFP^+ cells compared to the
175 control groups. siRNAs targeting gRNA and sgRNAs strongly suppressed GFP
176 expression until 40h p.i. (as they also targeted the GFP-transcript; Supplementary Fig.
177 2b,c) but then, the number of GFP^+ cells increased exponentially (Supplementary Fig.
178 2d,e). In contrast, groups treated with ORF1-specific siRNAs inhibited viral spread more
179 efficiently, showing a linear and generally slower increase of GFP^+ cells. In summary, our
180 data show that siRNAs which solely target SARS-CoV-2 gRNA subdue viral replication
181 more efficiently as compared to siRNAs that target additionally sgRNAs.

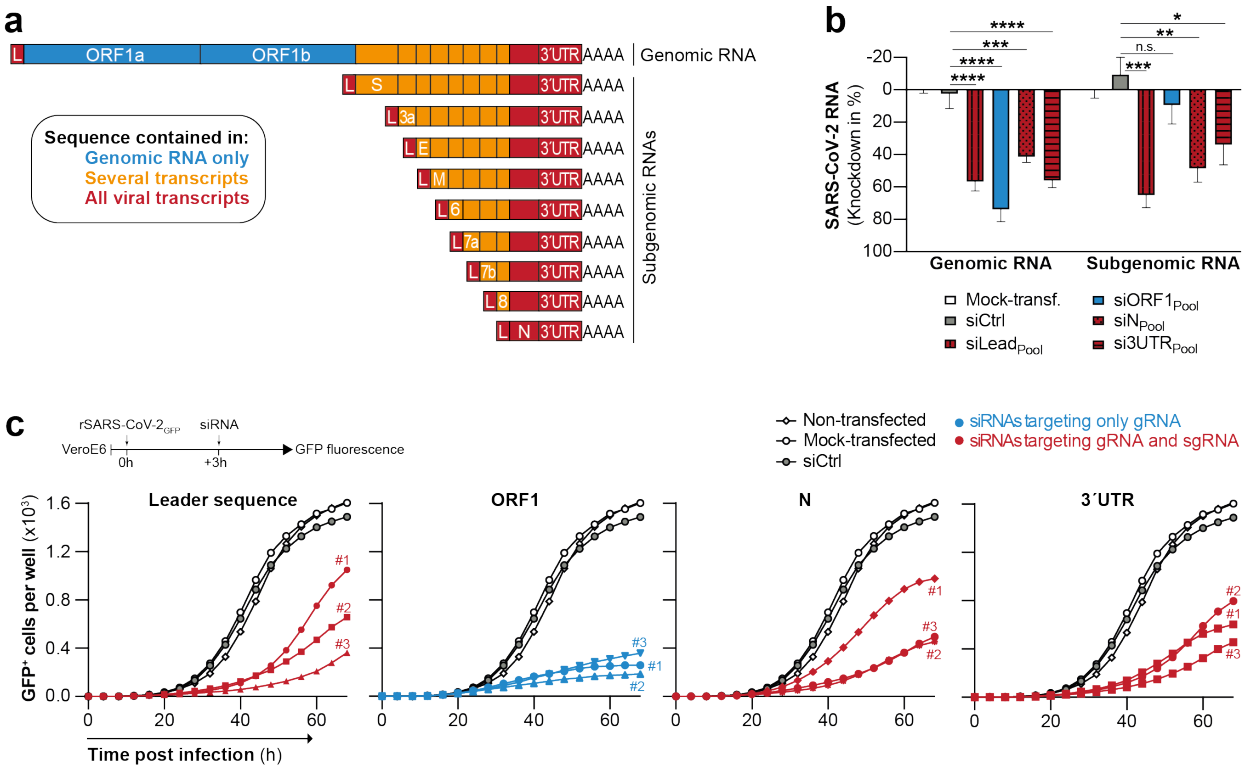

Fig.3 | Effect of targeting ORF1 or common sequences of SARS-CoV-2 transcripts with siRNAs. a, Schematic presentation of SARS-CoV-2 transcripts with sequences that are found in several transcripts shown in orange or red. Adapted from Kim et al. *Cell* 2020. **b**, Effect of siRNAs targeting ORF1 which is only part of full-length SARS-CoV-2 gRNA (blue) or targeting sequences common within gRNA and sgRNAs (red). VeroE6 cells were infected with *wildtype* SARS-CoV-2 and 3h p.i. transfected with siRNA pools (containing three siRNAs each) specific for indicated genomic regions of SARS-CoV-2. 24h p.i., viral gRNA and sgRNAs were quantified by RT-qPCR. gRNA levels are shown relative to 18s RNA and sgRNA relative to gRNA. **c**, VeroE6 cells were infected with rSARS-CoV-2-GFP and 3h p.i. transfected with siRNAs targeting indicated genomic regions of SARS-CoV-2 and GFP⁺ cells quantified every 4h. Each dot represents mean of three wells for each siRNA as indicated by number. Bar in **b** shows mean +/- SEM. Statistical difference were calculated using One-Way Anova with Dunette´s multiple comparision correction. n.s., non significant; *, $p<0.05$; **, $p<0.01$; ***, $p<0.001$; ****, $p<0.0001$

To investigate which replication step was more efficiently targeted by ORF1-specific siRNAs, we compared transfection of siRNAs before and after infection with *wildtype* SARS-CoV-2 and assessed viral RNA knockdown after 24h. While ORF1-specific siRNAs showed a trend towards slightly stronger efficacy compared to siRNAs targeting common regions when transfected after infection, the difference was significantly enhanced when siRNAs were transfected before infection (Supplementary Fig. 3). This indicated that ORF1-specific siRNAs had an advantage while targeting an early replication step of SARS-CoV-2. To further pinpoint which replication step was primarily affected, we transfected VeroE6 cells 6h before infection with *wildtype* SARS-CoV-2 and analyzed the effect on viral RNAs at different time points. Indeed, ORF1-specific siRNAs showed an

205 enhanced knockdown of gRNA already 1h p.i. (Fig. 4a) leading to decreased transcription
206 of negative sense gRNA (Fig. 4b) and sgRNAs (Fig. 4c). Taken together, our data
207 demonstrates that ORF1-specific siRNAs more efficiently targeted SARS-CoV-2 gRNA,
208 ergo, more efficiently prevented transcription, than siRNAs targeting common regions of
209 transcripts.
210 We hypothesized, that a second reason for the decreased efficacy of siRNAs targeting
211 gRNA as well as sgRNA could be that the high abundance of sgRNAs outcompeted
212 siRNAs and/or RNA-induced Silencing Complexes (RISC). To test this hypothesis, we
213 co-transfected siRNAs targeting the different SARS-CoV-2 regions together with their
214 respective luciferase reporter. After 6h, we infected cells with *wildtype* SARS-CoV-2 and
215 analyzed how SARS-CoV-2 replication in cells would affect silencing of the luciferase
216 reporter (Fig. 4d). Of note, in this experimental setting, both SARS-CoV-2 RNAs and
217 mRNA transcribed from a luciferase reporter plasmid can be targeted by the respective
218 siRNAs. Indeed, we found that silencing of luciferase reporters by siRNAs which targeted
219 gRNA and sgRNAs was significantly impaired by SARS-CoV-2 replication. This was not
220 observed for the ORF1-specific siRNA which suppressed the luciferase reporter with
221 same efficacy in both, infected as well as non-infected cells (Fig. 4e). In summary, our
222 data show that two mechanisms, a more efficient targeting of viral genomes by ORF1-
223 specific siRNAs, as well as an impaired RNAi silencing affecting siRNAs targeting
224 additionally sgRNAs, are responsible for the observed differences of siRNA activities.

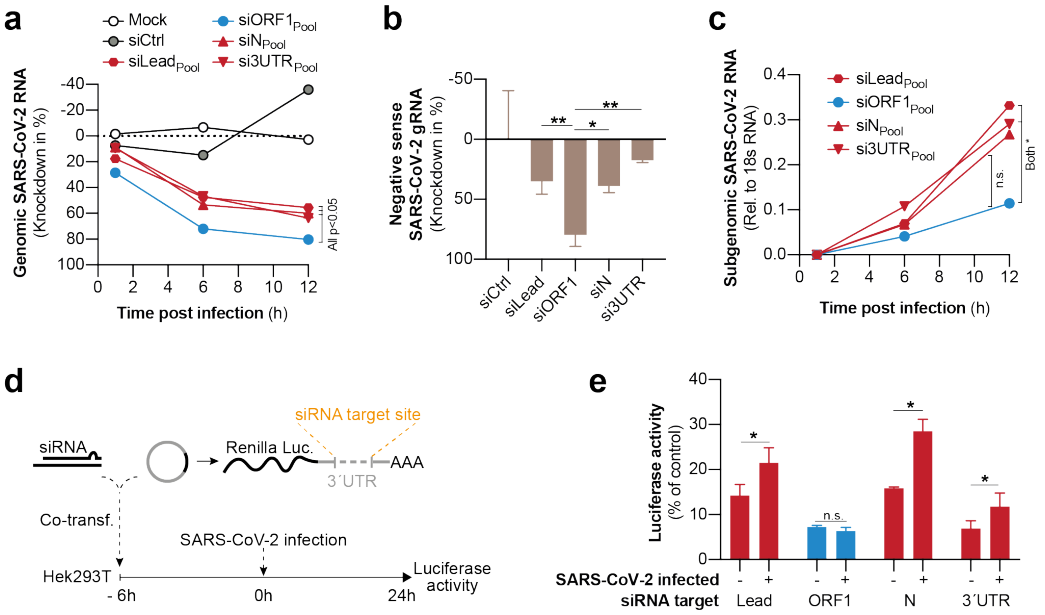

Fig. 4 | Mechanism of enhanced antiviral efficacy of siRNAs targeting ORF1. a-c, VeroE6 cells were transfected with siRNA pools against indicated target regions, 6h later infected with *wildtype* SARS-CoV-2 and viral RNAs quantified from cell lysates by RT-qPCR. **a**, Kinetic of total (containing positive and negative sense) gRNA at indicated time points. **b**, Negative sense gRNA quantified 6h p.i.. **c**, Kinetic of total (containing positive and negative sense) sgRNAs at indicated time points. **d-e**, Competition experiment to determine effect of SARS-CoV-2 replication on RNAi silencing efficacy. **d**, Human Embryonic Kidney (HEK) 293T cells were co-transfected with siRNAs against different target region as well as luciferase reporters with incorporated binding sites for the co-transfected siRNA. After 6h, cells were infected with *wildtype* SARS-CoV-2 and (**e**) luciferase activity determined from cell lysate 24h p.i.. Statistical differences were calculated using (**a,c**) Repeated Measures or (**b**) regular One-Way Anova with Dunette´s multiple comparison correction and (**e**) Student T-test for independent samples,. n.s., non significant, *, p<0.05; **, p<0.01

Discussion

A promising approach to develop antiviral therapies against SARS-CoV-2 constitute siRNAs, which is pursued by several academic and industry groups[32,33]. We provide the first proof that SARS-CoV-2 replication and spread can be efficiently controlled using siRNAs. We found that siRNAs, when given in a prophylactic setting, can target the genome of SARS-CoV-2 after cell entry and terminate replication before start of transcription. To our surprise, targeting solely gRNA resulted in a stronger antiviral efficacy than a simultaneous targeting of gRNA and sgRNA. We show that two independent mechanisms were responsible for this. First, ORF1-specific siRNAs more efficiently targeted genomes of SARS-CoV-2 before start of transcription. As ORF1 is the only translational active region before formation of RTC and ROs, the other genomic regions were probably less accessible for the RNAi machinery, due to secondary RNA structures[34] or as they are shielded by nucleocapsid proteins[35]. Second, the impaired

251 RNAi silencing affecting siRNAs targeting gRNA and sgRNAs could result from the high
252 abundance of sgRNAs outcompeting siRNAs and/or RISC complexes. This notion
253 appears especially plausible as Kim et al. showed that roughly 2/3rd of the transcriptome
254 of infected cells are made up of SARS-CoV-2 RNAs of which almost all contain the
255 targeted sequences[7]. Our findings on a first look might contradict a previous report which
256 described that targeting the leader sequence of SARS-CoV-1 with siRNAs would be more
257 efficacious than targeting the S ORF[16]. Several factors could explain differences found in
258 our study. First of all, SARS-CoV-1, which – while being the closest related virus – has
259 an amino acid sequence homology of only between 40-94% depending on the ORF[36],
260 thus findings might not be applicable to SARS-CoV-2. Also, Li et al. compared an siRNA
261 targeting the Leader sequence to siRNAs targeting the S gene, but not to ORF1-specific
262 siRNAs. As we speculate that one possible mechanism for the enhanced efficacy of
263 ORF1 siRNA stems from ORF1 being the only translational active region before start of
264 transcription, our finding might not apply to siRNAs targeting the S ORF. Third, Li et al.
265 compared only a single Leader-specific siRNA to two S-specific siRNAs questioning if the
266 finding can be generalized to the target region or if intra-individual differences of siRNA
267 activity were responsible for the observed differences. Regarding the reason why
268 negative sense SARS-CoV-2 RNA was not accessible for siRNA-silencing, the most
269 plausible explanation to us is that negative sense RNA – in contrast to positive sense
270 RNAs – are not exported from ROs. As probably no RISC complexes are present within
271 the ROs, activity of siRNA is restricted to RNAs which have either not yet entered ROs
272 (gRNA of incoming virus) or positive sense sgRNAs which are exported from ROs for
273 translation. This is in line with the notion that negative sense RNAs are not translated to
274 proteins, creating no necessity to export them into cytosol.
275 Several factors that have to be considered for clinical application were not addressed in
276 our study. During siRNA design, we did not take the conservation of target regions into
277 account which could affect occurrence of resistance mutations under therapy. However,
278 as ORF1 shows a relatively high conservation compared to other regions of the SARS-
279 CoV-2 genome[37], it appears plausible that an ORF1-specific siRNA drug candidate with
280 a high resistance barrier could be developed. Also, we did neither chemically modify our
281 siRNAs – which might further enhance activity, stability and tolerability of siRNAs – nor

282 did we use advanced delivery methods which would enhance efficacy an allow clinical
283 application[38-41].
284 To our knowledge, there is so far no equally detailed analysis of RNAi-targetable
285 replication steps and RNA species for any positive sense RNA virus. Thus, our results
286 might also be of relevance beyond SARS-CoV-2. Our finding that targeting SARS-CoV-2
287 gRNA reduced cytopathy could play out crucial as endothelial injury caused by viral
288 replication has been proposed to trigger pathology in lethal COVID-19 cases[11]. Along this
289 line, early therapy start or possibly even prophylactic application of siRNAs appears as
290 major benefit. Especially in this setting, targeting ORF1 was advantageous over targeting
291 sequences contained also in sgRNAs which could be a valuable information for designing
292 siRNAs and treatment regimens in clinical studies. Taken together, our study confirms
293 that siRNA-based strategies could allow to develop potent antivirals to reduce pathology
294 of COVID-19, encouraging academia and industry to proceed with ongoing efforts.

295 **Materials and Methods**

296

297 **siRNA design and synthesis**

298 The siRNAs used in the study were designed using siDirect (http://sidirect2.rnai.jp) and
299 siSPOTR (https://sispotr.icts.uiowa.edu/sispotr/index.html) online tools[42-44], structured
300 upon guidelines delineated from previous findings[45-48]. We designed siRNAs against four
301 regions of the SARS-CoV-2 genome: Leader sequence, ORF1, Nucleocapsid (N) and 3'
302 untranslated region (3'UTR), based on the full genome reference sequence available on
303 RefSeq database (NCBI Accession number: NC_045512.2). The siRNAs were designed
304 with an asymmetric design[42] and occasional G:U wobbles in 5' terminal of siRNA:mRNA
305 interaction[49] for improved specificity. Two additional siRNAs targeting GFP and Firefly
306 Luciferase were designed as negative controls. The luciferase-specific siRNA served as
307 control for infection experiments and the GFP-specific siRNA for experiments in which
308 Luciferase reporters were used. The siRNAs were purchased in desalted form from
309 Microsynth AG (Balgach, Switzerland), resuspended and maintained in RNAse free water
310 upon arrival. Activity of siRNAs was tested using luciferase reporters (see below) before
311 proceeding to the SARS-CoV-2 infection models.

312

313 **Cell lines and seeding**

314 HEK293T cells were maintained in glucose-containing Dulbecco's Modified Eagles
315 Medium (DMEM), supplemented with 10% Fetal Bovine Serum (FBS), 2mM L-Glutamine,
316 50U/ml Penicillin/Streptomycin, 1% Non-essential Amino acids, and 1mM Sodium
317 Pyruvate (Gibco™- Thermo Fisher Scientific GmbH; Dreieich, Germany). VeroE6 cells
318 were maintained in glucose-containing DMEM supplemented with 5% FBS. Mycoplasma
319 contaminations were excluded from all cell lines. Cells were kept at 37°C in humidified
320 incubators at 5% CO2. 200,000 HEK293T cells were plated in poly-L-lysin (Sigma-Aldrich
321 Chemie; Taufkirchen, Germany) treated 24-well plates for reporter assays, 700,000,
322 150,000, or 20,000 VeroE6 cells were plated in 6-well, 24-well, or 96-well plates (Techno
323 Plastic Products; Trasadingen, Switzerland) respectively for experiments including
324 SARS-CoV-2 infection.

325

326 **Cloning of luciferase reporters**

327 Initial siRNA screenings, testing of siRNA strand-specific activities and the competition
328 assay (shown in Supplementary Fig. 4d) were performed using the dual luciferase
329 expressing psiCHECK™-2 vector (Promega GmbH; Walldorf, Germany) with siRNA
330 target sites cloned into a multiple cloning site present downstream of the Renilla luciferase
331 translational stop codon. Thus, the full-length SARS-CoV-2 leader sequence and N gene
332 as well as the individual siRNA binding sites of siRNAs targeting ORF1 and the 3'UTR
333 were inserted by cloning via XhoI/NotI digestion (FastDigest™, Thermo Fisher Scientific;
334 Dreieich, Germany), according to manufacturer's instruction. The siRNA binding sites and
335 the Leader sequence were purchased as desalted ssDNA oligonucleotides with
336 overhangs mimicking digested oligonucleotide fragments and annealed *in vitro*. Hence,
337 equal amounts of respective complementary fragments were mixed and heated at 95 °C
338 for five minutes followed by gradual cooling for 2h at reduced temperatures. Resulting
339 annealed oligo-duplexes were directly used in a ligation reaction with the digested blank
340 psiCHECK-2™ vectors. The N gene was PCR amplified from cDNA of SARS-CoV-2
341 infected VeroE6 cells and first cloned into the pcDNA1/Amp plasmid vector. The cloned
342 plasmids were transformated into *E. coli* Stbl3 competent cells followed by plasmid
343 extraction (GeneJet™, Thermo Fisher Scientific; Dreieich, Germany). The resulting
344 recombinant vectors were confirmed by sequencing.

345

346 **Transfection**

347 siRNAs were either transfected 6h before or 3h after SARS-CoV-2 infection using
348 Lipofectamine RNAiMAX (Thermo Fisher Scientific; Dreieich, Germany). A final
349 concentration of 50 nM siRNA was used per well. For transfections before SARS-CoV-2
350 infection, a reverse-transfection protocol was used. Whereas, for transfections after virus
351 infection, a conventional forward-transfection protocol was employed – both according to
352 the manufacturer's instructions. All transfection experiments were performed with at least
353 three biological replicates. For the pre-selection of siRNAs, the determination of strand
354 specific activities of N-specific siRNAs, and the competition assay, siRNAs were co-
355 transfected together with respective plasmid expressing a luciferase reporter. In brief, 200
356 ng of reporter plasmid and 6 pmol of siRNA were mixed with 1 µl of transfection reagent

357 (Lipofectamine 2000, Thermo Fisher Scientific; Dreieich, Germany) diluted with Opti-
358 MEM to a final volume of 100 µl. siRNA-plasmid containing transfection complexes were
359 added on top of confluent cells, resulting in 10 nM final concentration of siRNA per well.
360 For the pre-screening of siRNAs and the determination of strand specific activities of N-
361 specific siRNAs, constructs were transfected into 85-90% confluent HEK293T cells and
362 for the competition assay into confluent VeroE6 cells.
363
364 **Dual-Luciferase based reporter assay and competition experiment**
365 As a surrogate model to determine siRNA activity, siRNAs were co-transfected into cells
366 with plasmids expressing dual luciferase reporters. After co-transfecting siRNAs and
367 plasmids (for details see paragraph above), cells were lysed after 48h (siRNA
368 prescreening and strand specific activities) with 100 µl Passive Lysis Buffer (Promega
369 GmbH; Walldorf, Germany), and luciferase activity from 10 µl cell lysate measured using
370 the Dual Luciferase® Reporter Assay System (Promega GmbH; Walldorf, Germany)
371 according to instructions using a Tecan Infinite 200 PRO Microplate reader (Tecan Group
372 Ltd.; Männedorf, Switzerland). Relative activity of *Renilla* luciferase (normalized to Firefly
373 luciferase activity as an internal transfection control) was indicated as silencing efficiency
374 of the siRNA and compared with a control siRNA targeting GFP or Luciferase. For the
375 competition experiment (shown in Fig. 4d-e), siRNAs and the respective luciferase
376 reporter plasmid were co-transfected into VeroE6 cells as described previously, which
377 were 6h later infected with *wildtype* SARS-CoV-2 (MOI 0.1) and 24h later luciferase
378 activity and knockdown efficacy were determined.
379
380 **SARS-CoV-2 infection**
381 VeroE6 cells were seeded in 24-well format at least 6h before infection to gain
382 approximately 90-95% confluency at time of infection. The SARS-CoV-2 stock was pre-
383 diluted for a multiple of infection (MOI) of 0.1 in 100µl media. At time of infection, old
384 growth media was removed and the pre-diluted SARS-CoV-2 solution added to cells.
385 After 1h incubation at 37°C, a medium exchange was performed. Different termination
386 time points were performed from 1 to 24h post infection based on the investigated step
387 of the viral replication cycle. The SARS-CoV-2 *wildtype* virus used in this study was

388 isolated from a patient in March 2020 at Institute of Virology, TU Munich. The full-length
389 sequence was uploaded onto GISAID database (https://www.gisaid.org/) under name
390 *hCoV-19/Germany/BAV-PL-virotum-nacq/2020* and accession ID: EPI_ISL_582134.
391
392 **Real-time monitoring of virus spread using rSARS-CoV-2-GFP and automated**
393 **fluorescence analysis with the IncuCyte® Live-Cell Analysis**
394 VeroE6 cells in growth media were seeded at least 6h before infection into 96-well plates
395 to gain approximated 90-95% confluency at time of infection. The rSARS-CoV-2-GFP
396 virus infection solution was pre-diluted for a MOI of 1 in 50µl growth media. After adding
397 50µl of the infection solution to cells, media was exchanged after 1h and multi-well plates
398 placed into IncuCyte® Live-Cell Analysis machine and phase contrast as well as
399 fluorescence pictures of the whole well acquired every 4h for three days. Total cell amount
400 (Phase channel) and infected cell population (GFP channel) were determined by the
401 IncuCyte S3 software (Essen Bioscience; version 2019B Rev2).
402
403 **Determination of cell viability**
404 The cell viability was determined using the CellTiter-Blue Cell Viability Assay kit (Promega
405 GmbH, Walldorf, Germany) according to manufacturer's instructions. In brief, VeroE6
406 cells were reversely transfected in 96-well plate with siRNAs 6h before SARS-CoV-2
407 infection (MOI 1), and cell viability assessed at different time points. For this, CellTiter-
408 Blue reagent was diluted 1:5 with culture medium and applied to cells for 60 min at 37 °C.
409 A distinct color change was observed in the untreated controls in comparison to the empty
410 well controls. Conversion from resazurin to resorufin was analysed with fluorescence
411 filters 550 / 590 nm at a Tecan Infinite F200 (Tecan Group Ltd.; Männedorf, Switzerland).
412
413 **Nucleic Acid extraction and qPCR**
414 RNA from cultured cells was extracted with the NucleoSpin RNA kit (Macherey-Nagel;
415 Düren, Germany), and cDNA synthesized with the Superscript™ III First-Strand Synthesis
416 System (Thermo Fisher Scientific; Dreieich, Germany) according to manufacturer's
417 instructions. SARS-CoV-2 transcripts were amplified in subsequent qPCR using primers
418 specific to the N region, essentially covering all the viral transcripts or the RNA dependent

419 RNA polymerase (Rdrp) region, as a measure of gRNA. For quantification of viral RNAs,
420 a standard curve was constructed using plasmids with integrated Rdrp or N sequences.
421 Amount of sgRNA was calculated by subtracting the result of PCR reaction using Rdrp
422 primers from the one using N primers (as full-length gRNA is also detected by the N
423 primers). 18s rRNA was used as a reference gene for relative quantification. All
424 quantitative PCRs were performed on a LightCycler® 480 (Roche Holding AG; Basel,
425 Switzerland) using primers and cycling conditions shown in Supplementary Table 1.
426

427 **Strand-specific cDNA synthesis**

428 To individually determine negative or positive sense SARS-CoV-2 RNA, we specifically
429 transcribed RNA of a certain polarity to cDNA. For this, first strand synthesis was
430 performed from total RNA extracts using the SuperScript™ IV First-Strand Synthesis
431 System (Thermo Fisher Scientific; Dreieich, Germany) with primers specific either for
432 positive sense mRNA (Oligo$(dT)_{20}$ primers) or negative sense mRNA (Oligo$(dA)_{20}$
433 primers). To allow transcription of a house keeping gene also in the reaction transcribing
434 negative sense RNA, primers specific for the 18s rRNA gene (18s cDNA1-3;
435 Supplementary Table 1) were added to the reaction. A final concentration of 50 µM for all
436 primers combined were used for first strand synthesis reaction and viral RNAs quantified
437 by qPCR as described above.

438 **Supplementary Table1. Oligonucleotides and cycling conditions used during polymerase change reaction.** A
439 = Adenine; C = Cytosine; G = Guanine; T = Thymine; Rev = reverse; min = minute; s = second; RDRP = RNA-dependent
440 RNA polymerase
441

Primers	**Sequence (5'-3')**
Oligo$(dT)_{20}$	TTTTTTTTTTTTTTTTTTTT
Oligo$(dA)_{20}$	AAAAAAAAAAAAAAAAAAAA
18s cDNA 1	CCTTCCGCAGGTTCACCTAC
18S cDNA 2	CCTCCAATGGATCCTCGT
18S cDNA 3	TAATCATGGCCTCAGTTCCG
18s qPCR	Fw: AAACGGCTACCACATCCA Rev: CCTCCAATGGATCCTCGT
N qPCR	Fw: GACCCCAAAATCAGCGAAAT Rev: TCTGGTTACTGCCAGTTGAATCTG
RDRP qPCR	Fw:CGTCTGCGGTATGTGGAAAG Rev: TAAGACGGGCTGCACTTACA
PCR cycling conditions:	Initial Denaturation: 95°C 5 Min (Ramp rate 4.4) 45 Cycles: 95°C - 15 seconds (Ramp rate 4.4) 55°C - 10 seconds (Ramp rate 2.2) 72°C - 25 seconds (Ramp rate 4.4)

442 **Statistical Analysis**

443 Statistical analysis was performed with GraphPad Prism (version 8.4.3) for Mac. Normally
444 distributed samples were analyzed using student T-test for independent samples when
445 comparing two groups and with One-way Anova with Dunnett´s multiple comparison
446 correction when comparing three or more groups. Statistical differences of non-normally
447 distributed data were calculated for two groups using Mann-Whitney U or Kruskal-Wallis
448 with Dunn´s multiple comparison correction tests when comparing three or more groups.
449 p-values <0.05 were considered significant.

450

451 **Acknowledgement**

452 We thank Prof. Dr. Volker Thiel for providing the recombinant, GFP-expressing SARS-
453 CoV-2 virus, Theresa Asen for help with cell culture and Prof. Dr. Ulrike Protzer for
454 general support such as providing the *wildtype* SARS-CoV-2 virus.

455

456 **Conflict of interest**

457 T.M. is an ad Hoc advisor for VIR Biotechnology and received research grants by Alnylam
458 Pharmaceuticals and Gilead Sciences. M.F. is a consultant for Dr. Hönle AG.

459

460 **Funding**

461 This study was supported by a research grant of the Bavarian State Government by the
462 *Förderprogramm Corona-Forschung* and the Else Kroener-Research College `Microbial
463 triggers as cause of disease´ to T.M. and ERC consolidator grant (ERC-CoG ProDAP,
464 817798), the German Research Foundation (PI1084/5, TRR178/TP11 TRR 237/A07) and
465 the German Federal Ministry of Education and Research (COVINET) to A.P.

References

1 Kruse, R. L. Therapeutic strategies in an outbreak scenario to treat the novel coronavirus originating in Wuhan, China. *F1000Res* **9**, 72, doi:10.12688/f1000research.22211.2 (2020).

2 Ghosh, S., Firdous, S. M. & Nath, A. siRNA could be a potential therapy for COVID-19. *EXCLI J* **19**, 528-531, doi:10.17179/excli2020-1328 (2020).

3 Baldassarre, A. *et al.* Potential use of noncoding RNAs and innovative therapeutic strategies to target the 5'UTR of SARS-CoV-2. *Epigenomics* **12**, 1349-1361, doi:10.2217/epi-2020-0162 (2020).

4 Chowdhury, U. F., Shohan, M. U. S., Hoque, K. I., Beg, M. A., Siam, M. K. S. and Moni, M. A. Computational Approach to Design Potential siRNA Molecules as a Prospective Tool for Silencing Nucleocapsid Phosphoprotein and Surface Glycoprotein Gene of SARS-CoV-2. *bioRxiv* **pp. 2020.04.10.036335.** (2020).

5 Sola, I., Almazan, F., Zuniga, S. & Enjuanes, L. Continuous and Discontinuous RNA Synthesis in Coronaviruses. *Annu Rev Virol* **2**, 265-288, doi:10.1146/annurev-virology-100114-055218 (2015).

6 Enjuanes, L., Almazan, F., Sola, I. & Zuniga, S. Biochemical aspects of coronavirus replication and virus-host interaction. *Annu Rev Microbiol* **60**, 211-230, doi:10.1146/annurev.micro.60.080805.142157 (2006).

7 Kim, D. *et al.* The Architecture of SARS-CoV-2 Transcriptome. *Cell* **181**, 914-921 e910, doi:10.1016/j.cell.2020.04.011 (2020).

8 Wölfel, R. *et al.* Virological assessment of hospitalized patients with COVID-2019. *Nature* **581**, 465-469, doi:10.1038/s41586-020-2196-x (2020).

9 Sungnak, W. *et al.* SARS-CoV-2 entry factors are highly expressed in nasal epithelial cells together with innate immune genes. *Nat Med* **26**, 681-687, doi:10.1038/s41591-020-0868-6 (2020).

10 Chu, H. *et al.* in *Lancet Microbe* Vol. 1 e14-23 (2020).

11 Ackermann, M. *et al.* Pulmonary Vascular Endothelialitis, Thrombosis, and Angiogenesis in Covid-19. *N Engl J Med* **383**, 120-128, doi:10.1056/NEJMoa2015432 (2020).

12 Beigel, J. H. *et al.* Remdesivir for the Treatment of Covid-19 - Final Report. *N Engl J Med*, doi:10.1056/NEJMoa2007764 (2020).

13 Horby, P. *et al.* Effect of Dexamethasone in Hospitalized Patients with COVID-19: Preliminary Report. doi:10.1101/2020.06.22.20137273 (2020).

14 WHO_Solidarity_trial_consortium *et al.* Repurposed antiviral drugs for COVID-19; interim WHO SOLIDARITY trial results. doi:10.1101/2020.10.15.20209817 (2020).

15 Chow, M. Y. T., Qiu, Y. & Lam, J. K. W. Inhaled RNA Therapy: From Promise to Reality. *Trends in pharmacological sciences* **41**, doi:10.1016/j.tips.2020.08.002 (2020).

16 Li, T. *et al.* siRNA targeting the leader sequence of SARS-CoV inhibits virus replication. *Gene Ther* **12**, 751-761, doi:10.1038/sj.gt.3302479 (2005).

17 Shi, Y. *et al.* Inhibition of genes expression of SARS coronavirus by synthetic small interfering RNAs. *Cell Res* **15**, 193-200, doi:10.1038/sj.cr.7290286 (2005).

18 Nur, S. M., Hasan, M. A., Amin, M. A., Hossain, M. & Sharmin, T. Design of Potential RNAi (miRNA and siRNA) Molecules for Middle East Respiratory Syndrome Coronavirus (MERS-CoV) Gene Silencing by Computational Method. *Interdiscip Sci* **7**, 257-265, doi:10.1007/s12539-015-0266-9 (2015).

19 Li, B. J. *et al.* Using siRNA in prophylactic and therapeutic regimens against SARS coronavirus in Rhesus macaque. *Nat Med* **11**, 944-951, doi:10.1038/nm1280 (2005).

20 Tang, Q., Li, B., Woodle, M. & Lu, P. Y. Application of siRNA against SARS in the rhesus macaque model. *Methods Mol Biol* **442**, 139-158, doi:10.1007/978-1-59745-191-8_11 (2008).

21 Baldassarre, A. *et al.* (Preprints.org, 2020).
22 Chowdhury, U. F. *et al.* A Computational Approach to Design Potential siRNA Molecules as a Prospective Tool for Silencing Nucleocapsid Phosphoprotein and Surface Glycoprotein Gene of SARS-CoV-2. *bioRxiv*, 2020.2004.2010.036335, doi:10.1101/2020.04.10.036335 (2020).
23 Hoffmann, M. *et al.* SARS-CoV-2 Cell Entry Depends on ACE2 and TMPRSS2 and Is Blocked by a Clinically Proven Protease Inhibitor. *Cell* **181**, 271-280.e278, doi:10.1016/j.cell.2020.02.052 (2020).
24 Burkard, C. *et al.* Coronavirus cell entry occurs through the endo-/lysosomal pathway in a proteolysis-dependent manner. *PLoS Pathog* **10**, e1004502, doi:10.1371/journal.ppat.1004502 (2014).
25 Shang, J. *et al.* Cell entry mechanisms of SARS-CoV-2. *Proc Natl Acad Sci U S A* **117**, 11727-11734, doi:10.1073/pnas.2003138117 (2020).
26 Fehr, A. R. & Perlman, S. Coronaviruses: an overview of their replication and pathogenesis. *Methods Mol Biol* **1282**, 1-23, doi:10.1007/978-1-4939-2438-7_1 (2015).
27 Snijder, E. J. *et al.* A unifying structural and functional model of the coronavirus replication organelle: Tracking down RNA synthesis. *PLoS Biol* **18**, e3000715, doi:10.1371/journal.pbio.3000715 (2020).
28 van Hemert, M. J. *et al.* SARS-coronavirus replication/transcription complexes are membrane-protected and need a host factor for activity in vitro. *PLoS Pathog* **4**, e1000054, doi:10.1371/journal.ppat.1000054 (2008).
29 Chang, C. K., Hou, M. H., Chang, C. F., Hsiao, C. D. & Huang, T. H. The SARS coronavirus nucleocapsid protein--forms and functions. *Antiviral Res* **103**, 39-50, doi:10.1016/j.antiviral.2013.12.009 (2014).
30 Thi Nhu Thao, T. *et al.* Rapid reconstruction of SARS-CoV-2 using a synthetic genomics platform. *Nature* **582**, 561-565, doi:10.1038/s41586-020-2294-9 (2020).
31 Hagemeijer, M. C., Vonk, A. M., Monastyrska, I., Rottier, P. J. & de Haan, C. A. Visualizing coronavirus RNA synthesis in time by using click chemistry. *J Virol* **86**, 5808-5816, doi:10.1128/JVI.07207-11 (2012).
32 Vir Biotechnology, I. a. A. P., Inc. (BUSINESS WIRE, SAN FRANCISCO & CAMBRIDGE, Mass., 2020).
33 NEWSWIRE, P. (PR NEWSWIRE, https://www.prnewswire.com/news-releases/sirnaomics-advances-rnai-based-prophylactics-and-therapeutics-to-battle-sari-caused-by-2019-ncov-300993007.html, 2020).
34 Rangan, R., Zheludev, I. N. & Das, R. RNA genome conservation and secondary structure in SARS-CoV-2 and SARS-related viruses. *bioRxiv*, doi:10.1101/2020.03.27.012906 (2020).
35 Baric, R. S. *et al.* Interactions between coronavirus nucleocapsid protein and viral RNAs: implications for viral transcription. *J Virol* **62**, 4280-4287, doi:10.1128/JVI.62.11.4280-4287.1988 (1988).
36 Grifoni, A. *et al.* A Sequence Homology and Bioinformatic Approach Can Predict Candidate Targets for Immune Responses to SARS-CoV-2. *Cell Host Microbe* **27**, 671-680.e672, doi:10.1016/j.chom.2020.03.002 (2020).
37 Abbott, T. R. *et al.* Development of CRISPR as an Antiviral Strategy to Combat SARS-CoV-2 and Influenza. *Cell* **181**, 865-876.e812, doi:10.1016/j.cell.2020.04.020 (2020).
38 Weber, S., Zimmer, A. & Pardeike, J. Solid Lipid Nanoparticles (SLN) and Nanostructured Lipid Carriers (NLC) for pulmonary application: a review of the state of the art. *Eur J Pharm Biopharm* **86**, 7-22, doi:10.1016/j.ejpb.2013.08.013 (2014).
39 de Kruijf, W. & Ehrhardt, C. Inhalation delivery of complex drugs-the next steps. *Curr Opin Pharmacol* **36**, 52-57, doi:10.1016/j.coph.2017.07.015 (2017).

566 40 Feldmann, D. P. & Merkel, O. M. The advantages of pulmonary delivery of therapeutic
567 siRNA. *Ther Deliv* **6**, 407-409, doi:10.4155/tde.15.8 (2015).
568 41 Kandil, R. & Merkel, M. Therapeutic delivery of RNA effectors: diseases affecting the
569 respiratory system. *Pharmazie* **71**, 21-26 (2016).
570 42 Boudreau, R. L. *et al.* siSPOTR: a tool for designing highly specific and potent siRNAs
571 for human and mouse. *Nucleic Acids Res* **41**, e9, doi:10.1093/nar/gks797 (2013).
572 43 Naito, Y., Yamada, T., Ui-Tei, K., Morishita, S. & Saigo, K. siDirect: highly effective,
573 target-specific siRNA design software for mammalian RNA interference. *Nucleic Acids*
574 *Res* **32**, W124-129, doi:10.1093/nar/gkh442 (2004).
575 44 Naito, Y., Yoshimura, J., Morishita, S. & Ui-Tei, K. siDirect 2.0: updated software for
576 designing functional siRNA with reduced seed-dependent off-target effect. *BMC*
577 *Bioinformatics* **10**, 392, doi:10.1186/1471-2105-10-392 (2009).
578 45 Boudreau, R. L., Spengler, R. M. & Davidson, B. L. Rational design of therapeutic
579 siRNAs: minimizing off-targeting potential to improve the safety of RNAi therapy for
580 Huntington's disease. *Mol Ther* **19**, 2169-2177, doi:10.1038/mt.2011.185 (2011).
581 46 Reynolds, A. *et al.* Rational siRNA design for RNA interference. *Nat Biotechnol* **22**, 326-
582 330 (2004).
583 47 Ui-Tei, K., Naito, Y., Nishi, K., Juni, A. & Saigo, K. Thermodynamic stability and Watson-
584 Crick base pairing in the seed duplex are major determinants of the efficiency of the
585 siRNA-based off-target effect. *Nucleic Acids Res* **36**, 7100-7109,
586 doi:10.1093/nar/gkn902 (2008).
587 48 Ui-Tei, K. *et al.* Guidelines for the selection of highly effective siRNA sequences for
588 mammalian and chick RNA interference. *Nucleic Acids Res* **32**, 936-948,
589 doi:10.1093/nar/gkh247 (2004).
590 49 Holen, T. *et al.* Tolerated wobble mutations in siRNAs decrease specificity, but can
591 enhance activity in vivo. *Nucleic Acids Res* **33**, 4704-4710, doi:10.1093/nar/gki785
592 (2005).

593

Supplementary Figures

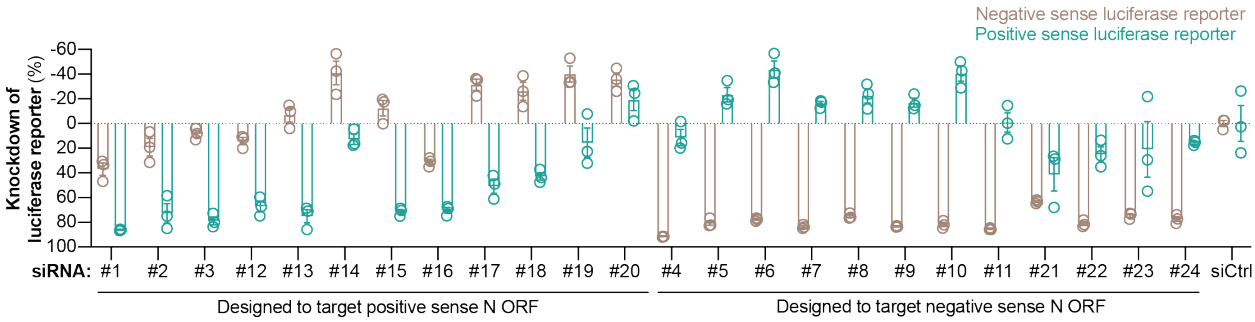

Supplementary Fig. 1 | Prescreening with luciferase reporters to identify siRNAs with selective activity against positive or negative sense N ORF. Hek293T cells were co-transfected with siRNAs and reporter plasmids expressing luciferase with either negative or positive sense N ORF cloned into the 3´UTR. 48h after transfection, cells were lysed and luciferase activity measured. Graph shows mean reduction of luciferase activity by the SARS-CoV-2 specific siRNA compared to the same reporter co-transfected with the control siRNA. siRNAs 1-11 were selected for further studies. Error bars indicate SEM.

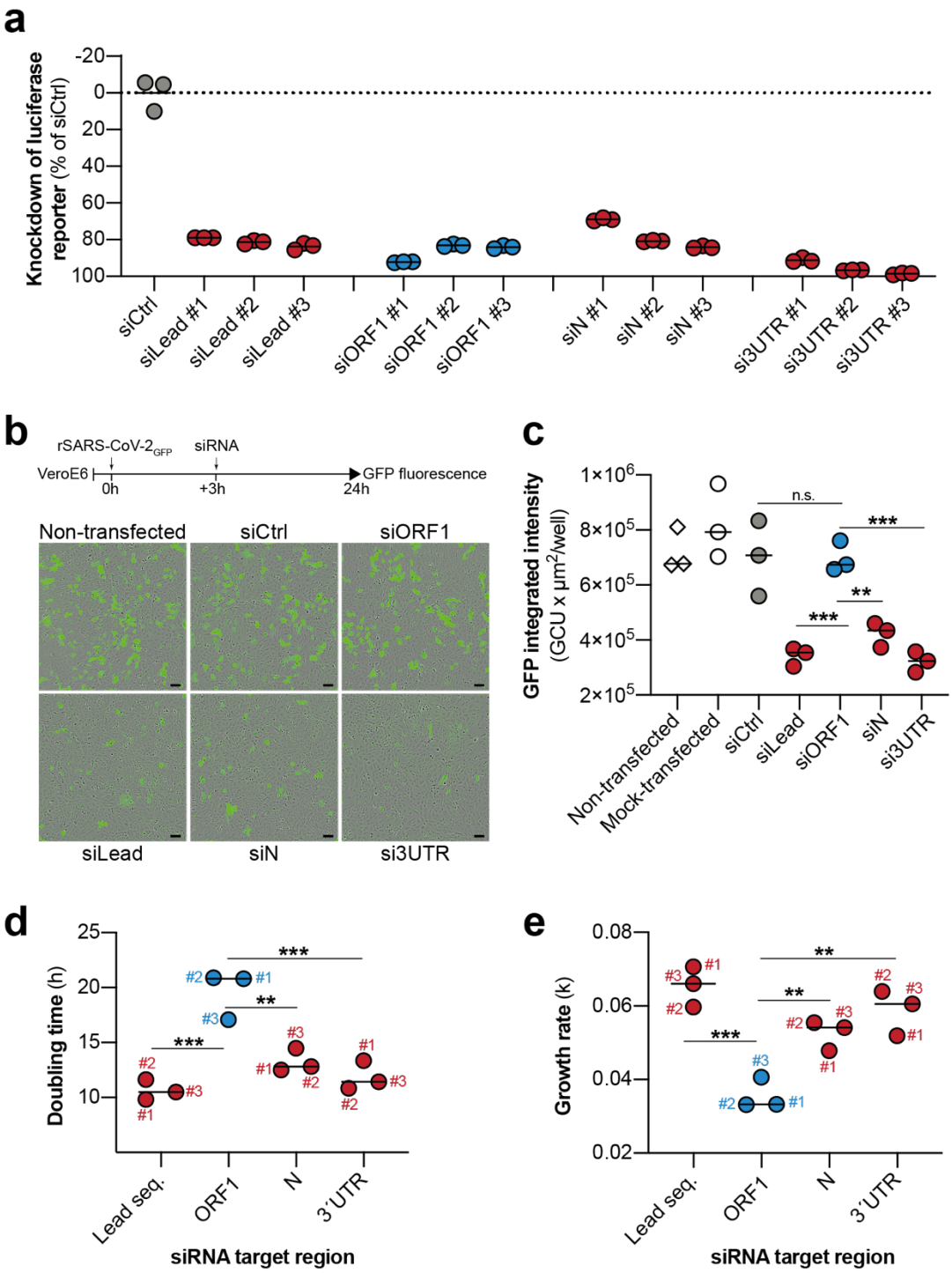

Supplementary Fig. 2 | ORF1-specific siRNAs have an enhanced effect on viral spread compared to siRNAs targeting common region of SARS-CoV-2 transcripts. a, Knockdown of luciferase reporters with incooroporated siRNA target sites by siRNAs used in this study. **b-c**, VeroE6 cells were infected with rSARS-CoV-2-GFP 3h before transfecting siRNAs against indicated target regions and GFP-intensity measured every 4h. **b**, Exemplary fluorescence microscopy pictures taken 24h after infection. **c**, Quantifcation using the Incucyte S3 analysis software. **d-e**, Increase of GFP$^+$ cells as a marker of virus spread was measured by fitting an exponential curve to graphs shown in Fig. 3c and (**d**) doubling time as well as (**e**) growth rate analyzed. Statistical differences were calculated using One-Way Anova with Dunnett´s multiple comparison correction. n.s., non significant; **, p<0.01; ***, p<0.001; ****, p<0.0001

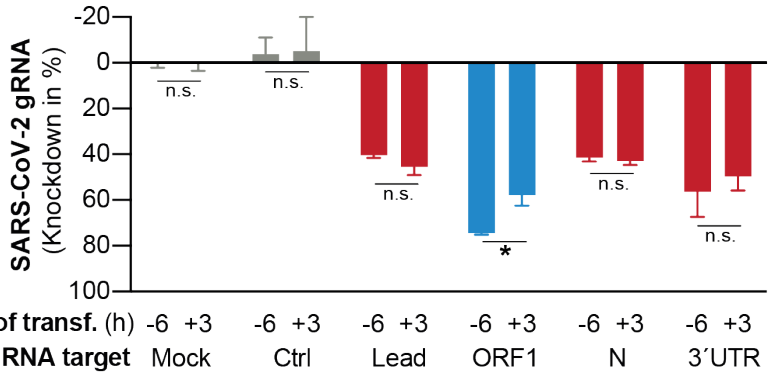

Supplementary Fig. 3 | ORF1-specific siRNAs show enhanced efficacy on early replication step. **a**, VeroE6 cells were transfected with siRNA pools against indicated target regions either 6h before, or 3h after infection with wildtype SARS-CoV-2. Viral gRNA was quantified (relative to 18S RNA) from cell lysates obtained 24h p.i. by RT-qPCR. Statistical differences were calculated using Student T-test for independent samples. n.s., non significant, *, $p<0.05$